

A Breakage-Stop System for Linen Wet Spinning Frame

Bo Jin^{*}, Lijun Zhao and Shiqiang Zhu

The State Key Lab of Fluid Power Transmission and Control, Department of Mechanical Engineering, Zhejiang University, Hangzhou, China, 310027

Abstract: A multi-way control system for spun yarn breakage detecting and tow stopping is presented for linen wet spinning frame upgrade in medium-sized businesses of southeastern China. The signals from periodic rotations of spun yarns are picked by piezoelectric sensors. After input protection and multiplexers, the weak voltage signal from gated channel is processed through links including voltage following, passive high-pass filter, active low-pass filter, in-phase and reversed-phase proportional amplifying, precision full-wave rectification, retardation voltage comparison, etc.. After regulated at a zener diode link, the final electrical level is sent to LPC2132 processor which gives trigger signals to actuators when yarn breakage is detected. In the corresponding actuator channel, armature of electromagnet will be pushed off to stop tow feed and the red LED will be lightened to warn spinner. Circuit board units for signal amplifying, conditioning and actuator driving were designed for controlling 24 yarn channels simultaneously. The simulation result and field test verified the circuit accuracy and programmed effectiveness.

Keywords: Automatic tow stopping, control system, linen wet spinning, yarn breakage detection.

1. INTRODUCTION

Yarn spinning is the last procedure in linen wet spinning [1]. According to certain quality standards or customers' requirements, coarse tow needs to be turned into twisted fine yarns for threads doubling, machine knitting or weaving [2, 3]. Only after coarse tow is drafted and twisted can the generated spun yarns be wound on spindles [4]. Due to the inevitable influence from neppiness and unevenness, breakage happens occasionally to twisted yarn [5, 6]. Then coarse tow feed should be stopped in time. Not until the broken twisted yarn is connected again can the coarse tow feed be restarted.

In some medium-sized textile plants of southeastern China, few mechanical or electric devices are equipped on the obsolete spinning frames for yarn breakage detection, stopping and warning as shown in Fig. (1). Yarn spinning courses are generally monitored manually, which lead to low breakage detection and disposal efficiency. So we developed an automatic system for the upgrading of linen wet spinning frames.

2. GENERAL DESCRIPTION OF THE SYSTEM

For spun yarn detection, existing approaches are based on capacitive, piezoelectric, photoelectric or laser principle [7, 8]. Capacitive sensor is quite mature [9, 10] but matched signal processing circuits needs to be highly sensitive. This leads to possible erroneous judgments caused by interference [11]. Photoelectric sensors are also non-contact and fast

responding, but they are more effective for grouped yarns [12-14]. Moreover, they are subject to dirt accumulation [15]. Laser-based methods need cameras for image grabbing and the processor requirement is higher due to image processing burden [16]. Considering installation space, signal processing circuit complexity and overall cost, we chose piezoelectric sensor as shown in Fig. (2a). It has excellent dynamic performance for measuring periodic motions [17]. In tow channels, integrated actuators, as shown in Fig (2b), are used which combine electromagnet for coarse tow stop and red LED for yarn breakage warning. The proposed control system is designed for monitoring 24 channels of yarns simultaneously. The block diagram is given in Fig. (3).

During yarn spinning, spindle rotation makes the tense spun yarn revolve at a frequency of about 100Hz. After being picked by piezoelectric sensor, the weak voltage signal generated by the revolving yarn is amplified in a series of circuits (Sect. 3). If yarn breakage happens, a high level will be generated and sent to the processor which will send trigger signal to actuators in the corresponding channel as a respond. Through power amplification circuit (Sect. 4), the armature on electromagnet will be pushed off to stop coarse tow feed and the LED will be lighted as warning.

After the breakage is disposed successfully, spinner resets the armature. When spun yarn existence is detected again from sensor, the red LED will be powered off automatically. The processor used in the proposed system is LPC2132 from NXP. It has plenty of user resources especially 47 GPIO ports which facilitates the circuit design in this work. Pin definition is given in Table 1 for the used GPIO ports because they are of complex function. Only P.20 is used for input, i.e., the other GPIO pins are used with output function.

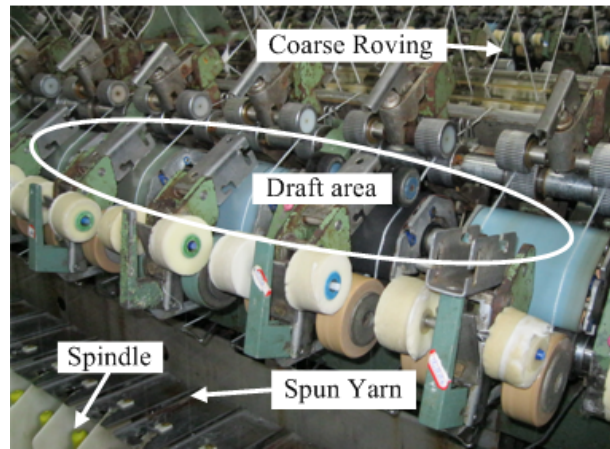


Fig. (1). Yarn spinning frame in operating.

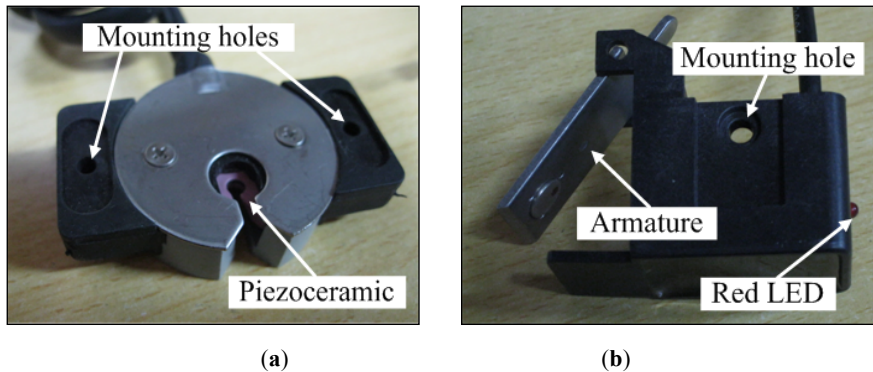


Fig. (2). Sensor and actuator adopted for the system.

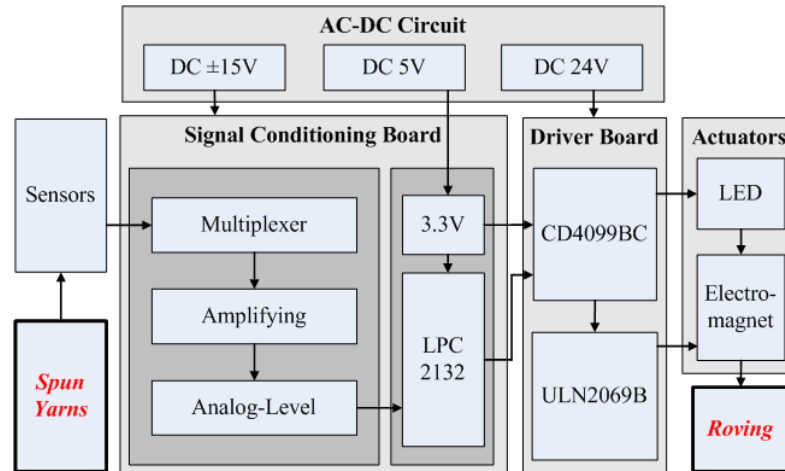


Fig. (3). Configuration of the control system.

3. SENSOR SIGNAL AMPLIFICATION AND CONTROLLER CIRCUITS

The spun yarn existence signal from piezoelectric sensor has low voltage amplitude, 10mV as maximum. A circuit for signal amplification is designed which contains a series of analog signal processing links as shown in Fig. (4).

Three chips of HFC4051 are used in block A for gating the 24 channels of sensors inputs (each chip for eight inputs). Thus the subsequent circuit is shared by all input channels. Additional GPIO and components consumption are avoided

while detection efficiency is not influenced. When treated as voltage source, piezoelectric sensors have large equivalent impedance. Voltage follower which has high input impedance and low output impedance is adopted in block B for signal buffer. We used JFET-input operational amplifier TL084CN here. Then passive first-order high-pass filter (cut-off frequency as 0.724Hz and pass-band gain as 1) in block C restrains DC and low-frequency interference. With the in-phase proportional amplifier in D with high input impedance, signal amplitude is magnified 11 times. After the second passive first-order high-pass filter (cut-off frequency as

Table 1. Definition for GPIO pins of LPC2132.

Pin Name	Function	Description
P0.0	Dis_1	Disable signals for 6 chips of CD4099BE
P0.1	Dis_2	
P0.2	Dis_3	
P0.3	Dis_4	
P0.4	Dis_5	
P0.5	Dis_6	
P0.6	A0	Address, data and clear data lines for CD4099BE (shared by 6 chips)
P0.7	A1	
P0.8	A2	
P0.9	D	
P0.10	CD	
P0.11	SW	Enable electromagnet
P0.12	En3CD	Enable CD4099BE for LED
P0.13	SW_A	Address lines for HCF4051
P0.14	SW_B	
P0.15	SW_C	
P0.16	Inhibit1	Chip select lines for 3 chips of HCF4051
P0.17	Inhibit2	
P0.18	Inhibit3	
P0.20	input	Level signal of sensor input

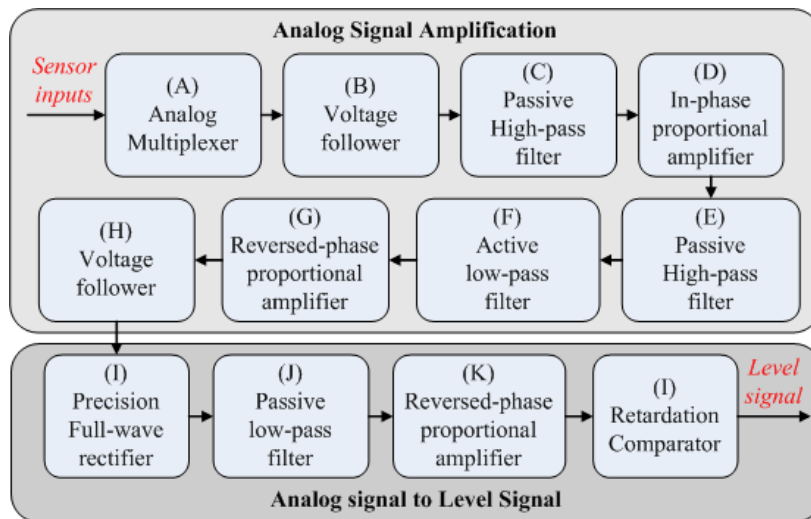


Fig. (4). Block diagram of sensor signal processing circuit.

6.12Hz) in E, possible DC or low-frequency interference are eliminated basically. Then through the fourth-order low-pass filter in F, high-frequency interferences are also eliminated.

As shown in Fig. (5), the fourth-order low-pass filter in F is implemented by using two active second-order low-pass

filters in series. The pass-band gain and cut-off frequency are designed as:

$$A_{up} = A_{up1} \cdot A_{up2} = \left(1 + \frac{R_{10}}{R_7}\right) \cdot \left(1 + \frac{R_{12}}{R_{13}}\right) = 2.65$$

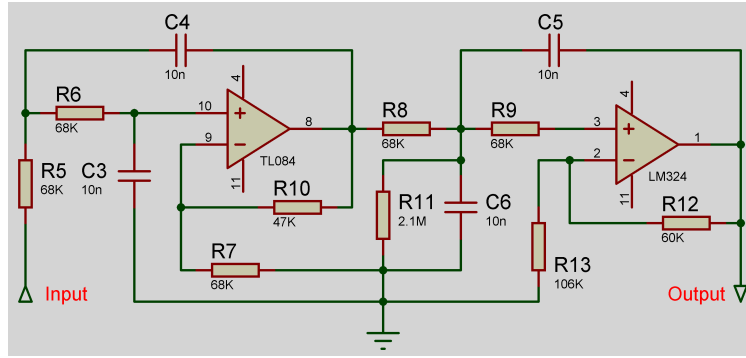


Fig. (5). Fourth-order low-pass filter.

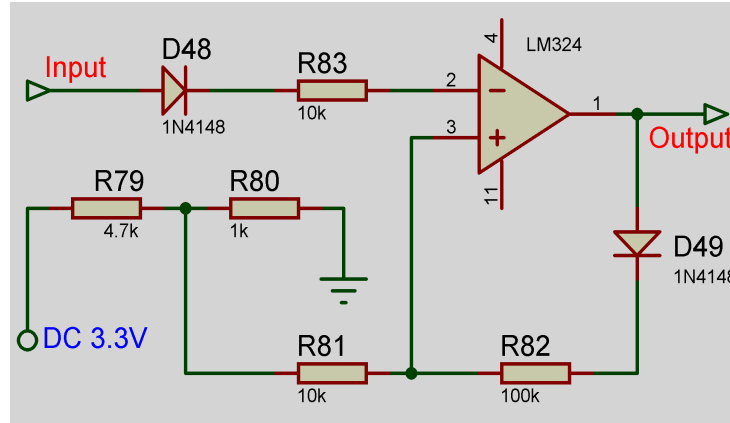


Fig. (6). Retardation Comparator.

$$f_p = f_{p1} = f_{p2} = \frac{1}{2\pi\sqrt{R_6 R_5 C_4 C_3}} = \frac{1}{2\pi\sqrt{R_9 R_8 C_6 C_5}}$$

$$= \frac{1}{2\pi \times 68 \times 10^3 \times 10 \times 10^{-6}} = 234.17\text{Hz}$$

In block G, the signal amplitude is enlarged 8.47 times using reversed-phase proportional amplifier. During the above seven steps, the signal always maintains a sinusoidal form. To obtain desired high-low-level signal, we used precision full-wave rectification in I after voltage following in H. The generated half-wave signal is magnified 40 times by reversed-phase proportional amplifier in step J and then smoothed by a passive first-order low-pass filter (cut-off frequency as 234.17Hz) in block K. Retardation comparing circuit is adopted in step L as anti-interference measure.

As shown in Fig. (6), a special structure is adopted for the retardation comparison circuit to obtain required outputs. One Schottky diode is used in the input terminal to prevent negative signal. Another Schottky diode is adopted instead of zener diode in the positive feedback branch. Reference voltage V_{ref} is given by using resistive subdivision at the terminal of R_{81} which is grounded in common retardation comparator.

$$V_{ref} = V_{VDD} \frac{R_{80}}{R_{79} + R_{80}} = 3.3 \frac{1}{4.7 + 1} \approx 0.6\text{V}$$

The two threshold voltage can be determined as:

$$u_{high} = U_{AP} \frac{R_{81}}{R_{81} + R_{82}} + V_{ref}$$

$$u_{low} = V_{ref}$$

Where, U_{AP} is the maximum output voltage of operational amplifier. LM324N is adopted in this link with $\pm 12\text{V}$ power supply, so we had $u_{high} \approx 1.6\text{V}$, $u_{low} = 0.6\text{V}$.

Finally, level signals are obtained after a simple zener diode stabilizing link and sent to the controller (Low level represents spun yarn existence while high level indicated yarn breakage). As illustrated in Fig. (7), for the controller, external crystal with 11.0592Hz frequency and DC 3.3V supply are given to LPC2132. For the purpose of stability and anti-interference, we adopted voltage regulator and power supply isolation as shown in Fig. (8).

4. DRIVING CIRCUIT FOR ACTUATORS

For the integrated actuators, the drive current for LED is about 10mA. We used three chips of 8-bit addressable latch (CD4099BC) to control 24 channels of LED in each spinning unit. The drop voltage of each LED is about 1.7V, and the output current of CD4099BC is about 0.88mA, so current limiting resistor value is determined as:

$$R_{lim} = \frac{U_V - U_L}{I_{IO}} = \frac{3.3 - 1.7}{0.88 \times 10^{-3}} \approx 1.8\text{K}\Omega$$

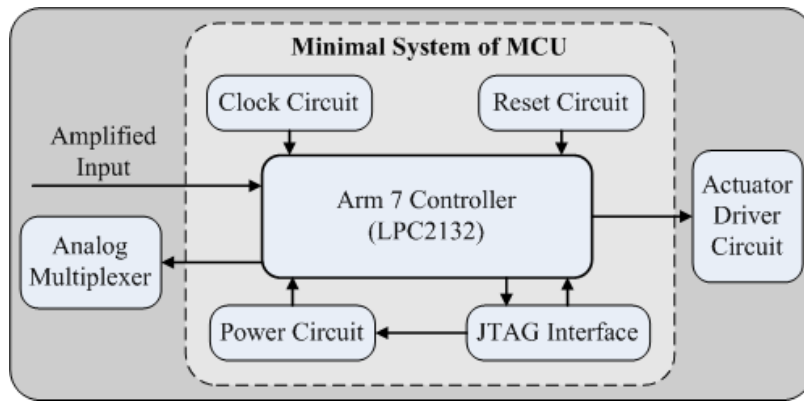


Fig. (7). Block diagram of the controller circuit.

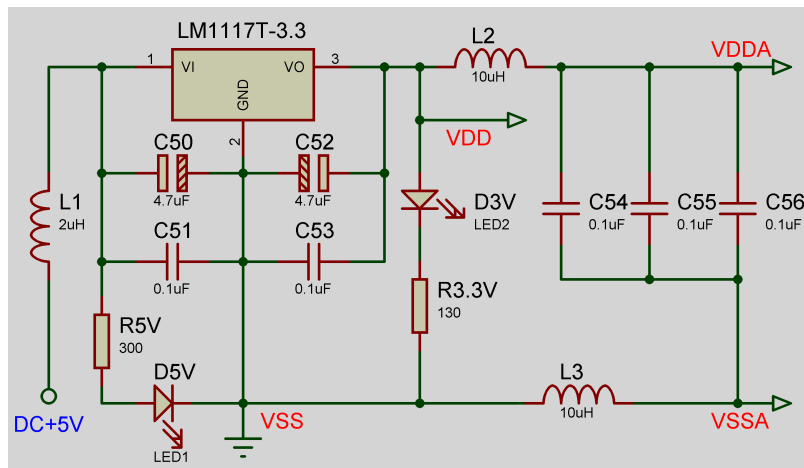


Fig. (8). Power supply circuit for the controller.

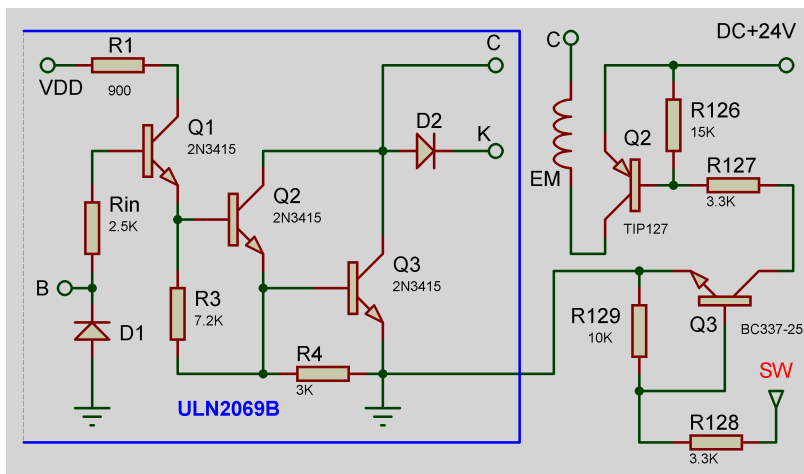


Fig. (9). Driver circuit for electromagnet.

For each electromagnet, drive current must be over 1.5A to push off the armature when spun yarn breakage is detected. We used quad Darlington switches (ULN2069B) which could provide current up to 1.75A. The structure of each Darlington switch is given in Fig. (9). The pins K and C are connected to one end of the electromagnet coil. DC supply (+24V) is connected to K through power transistor TIP127 (controlled by SW levels from LPC2132 through BC337). When high level is given to pin B, the Darlington switch will be turned on, and the voltage at pin C will be decreased significantly. The magnet coil puts off the armature and coarse

tow feed will be stopped. To control 24 channels of electromagnets, we used three chips of CD4099BC to give switch signals to six chips of ULN2069B.

5. PROGRAM DESCRIPTION

All the codes for signal acquisition, flow control and actuator driving are written with C language and debugged with the ADS v1.2 tools released by ARM Co. Ltd. Global variables are defined to facilitate programming (Table 2).

Table 2. Global variables used in main function.

Type	Name	Description
uint32	input_state	detected spun yarn state
uint32	current_state	last stored spun yarn state
uint8	number_output	count for 24 output channels
uint8	number_input	count for 24 input channels
uint32	Temp	temporary register

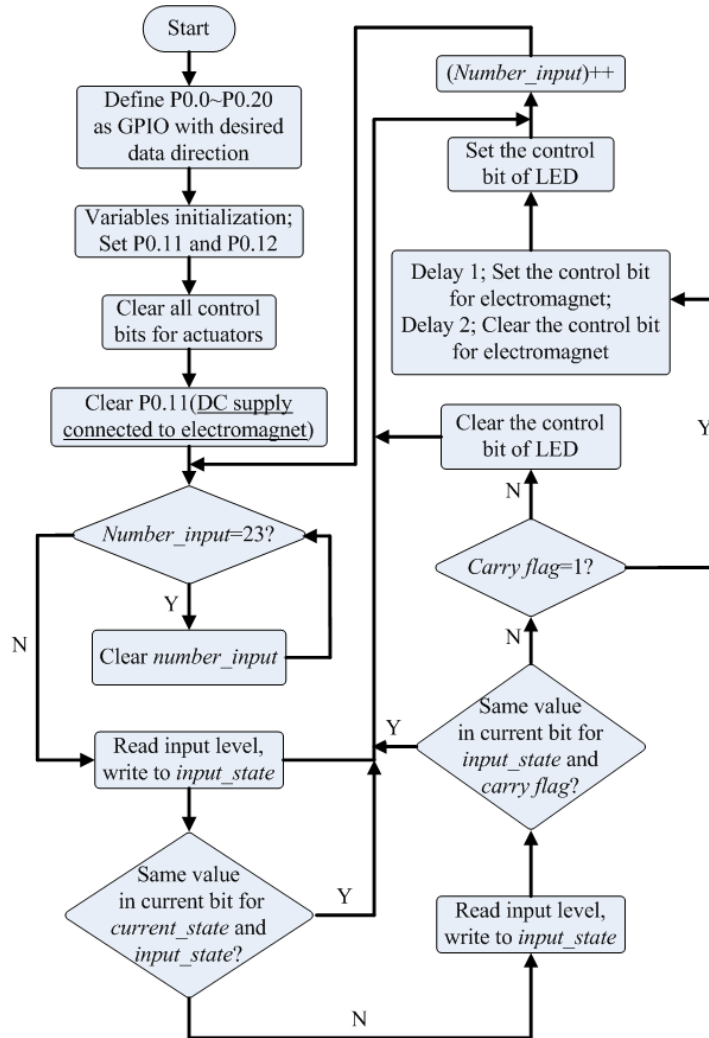


Fig. (10). Flow chart of the main function.

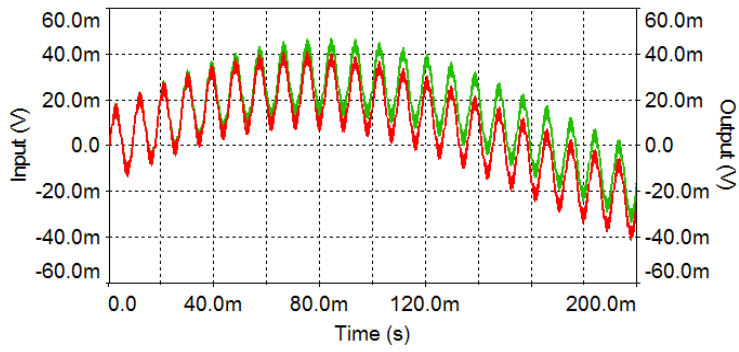
As shown in Fig. (10), after the detecting system is started, function definition is given to relevant GPIO pins (Table 1). Then default values are given to variables during initialization. After the control bits of all LED and electromagnet channels are cleared, enable signal is given to connect +24V power supply to electromagnets. Breakage detection begins to cycle for the 24 channels of yarn sensor inputs.

Especially, through the comparison of yarn state variable values, judgment of carry flag and time delay of armature

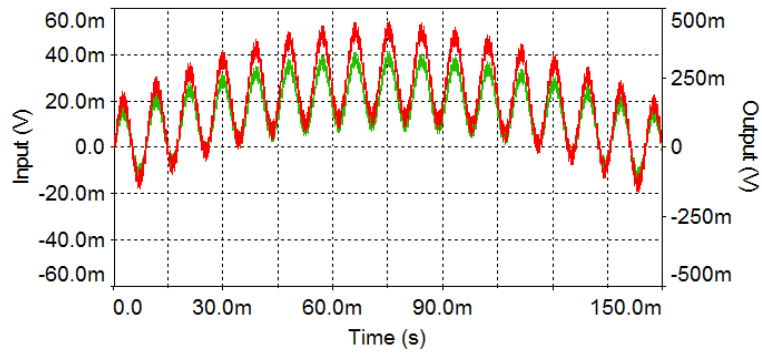
actuation, electromagnet malfunction is averted when spinner is connecting the spun yarn (intermittent signal could be generated by the touch between shaking spun yarn and sensor) and resetting the armature.

6. SIMULATION AND EXPERIMENT RESULTS

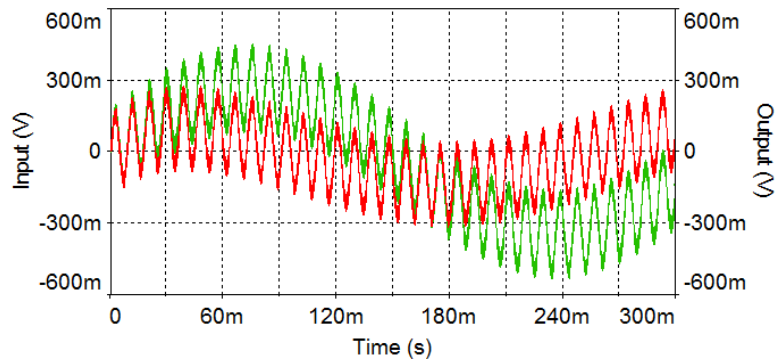
We simulated the processing circuit for sensor input in Multisim 11.0 platform. The first voltage following link,



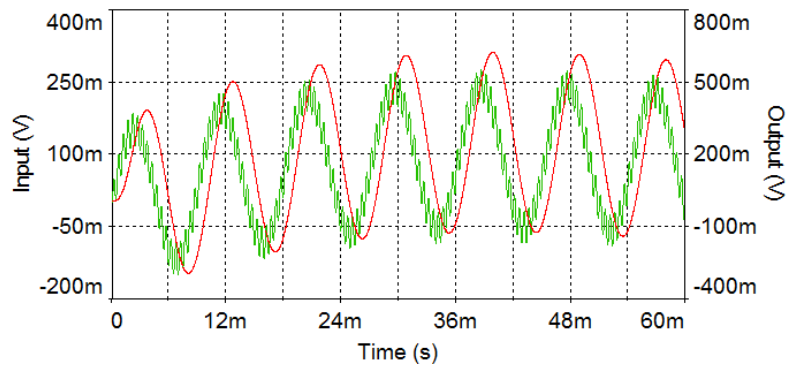
(a)



(b)

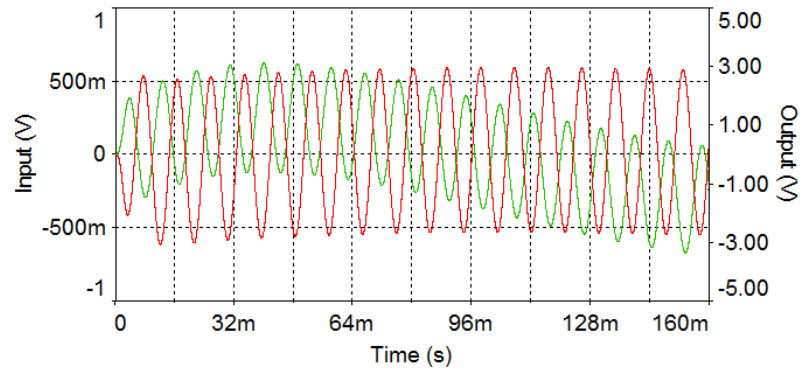


(c)

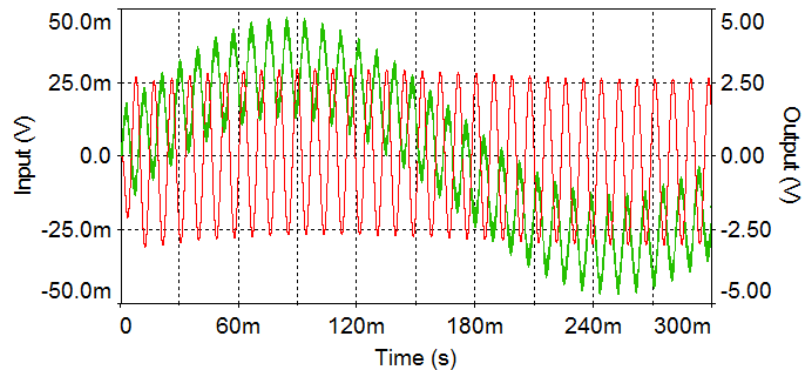


(d)

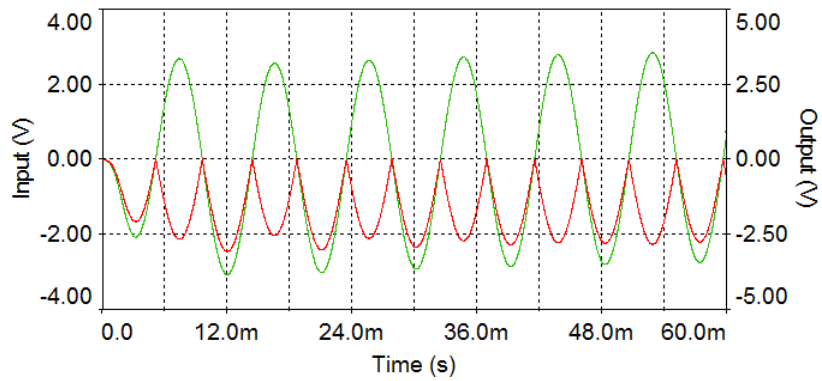
Fig. (11). Contd...



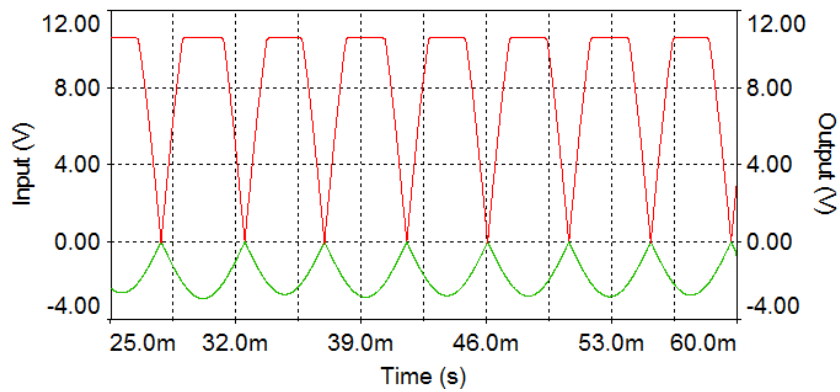
(e)



(f)



(g)



(h)

Fig. (11). Contd...

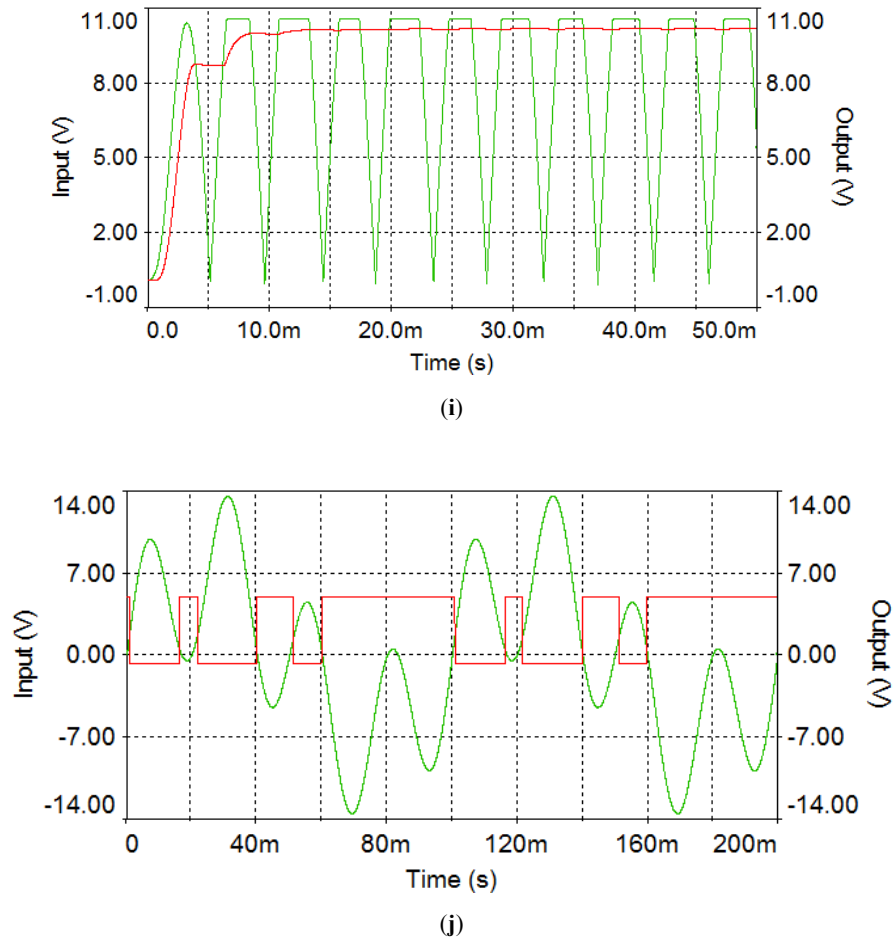


Fig. (11). Simulation results of signal amplification circuit.

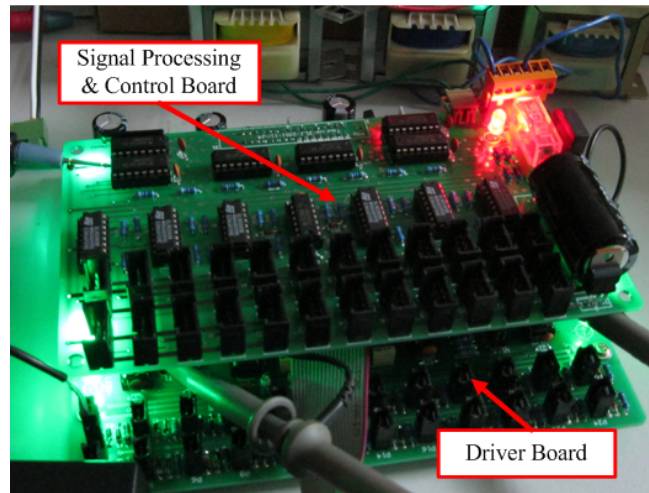
in-phase proportional amplifying step in Fig. (4) and the first active second-order low-pass filter in Fig. (5) are built based on JFET input operational amplifier TL084CN. The second low-pass filter in Fig. (5), reversed-phase proportional amplifying and voltage following links are based on LM324N. The component models adopted in the simulations are the same as those used on the PCB boards for field application. The supply voltage for TL084CN and LM324N are respectively set as $\pm 15\text{V}$ and $\pm 12\text{V}$.

The emulated input signal is the superposition of three sinusoidal waves including assumed sensor signal ($A = 10\text{mV}$, $f = 100\text{Hz}$), high-frequency interference ($A = 3\text{mV}$, $f = 2\text{KHz}$) and low-frequency interference ($A = 30\text{mV}$, $f = 3\text{Hz}$) as the green wave in Fig. (11a).

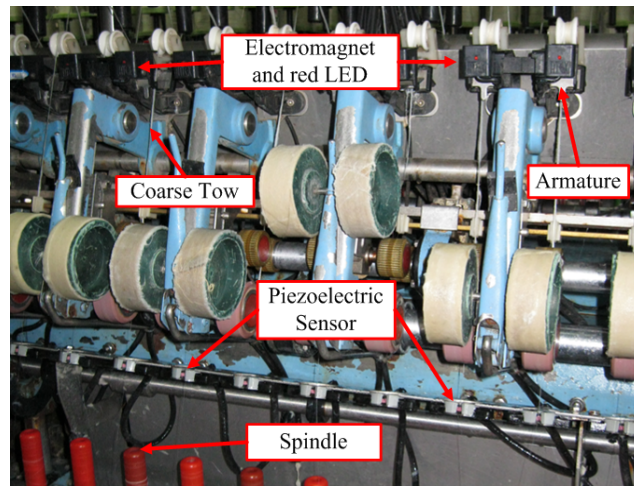
Corresponding to the blocks in Fig. (4), after the passive high-pass filter in C, the voltage waveforms are given in Fig. (11a). The green curve represents input signal and the red curve reflects output signals (the same for images in b-j). Amplitude and phase differences between the two waves indicate that low-frequency interference is not eliminated completely. That's because the cut-off frequency of the filter is 0.724Hz (close to 1Hz of low-frequency interference). To make all interferences eliminated in less than two filters is irrational because the weak sensor signal can be affected. The red wave in Fig. (11b) shows that the input signal is amplified 11 times through step D.

After the second passive high-pass filter in E, the low-frequency interference is eliminated mostly as shown in Fig. (11c). The low-pass filter effect of block F can be seen in Fig. (11d). The red wave which represents filtered signal has no ripple (amplitude enlarged 2.5 times). The reversed-phase proportional amplifier in G magnifies input signal 8.32 times as shown in Fig. (11e). Meanwhile, a capacitor (47nF) is used at the input terminal, so step G also has combined high-pass filter effect (cut-off frequency is 8.47Hz). In Fig. (11e), the slow fluctuating trend of green wave (input) disappeared in red wave (output). That means the low-frequency interference is completely eliminated.

After the last voltage following link in H, the amplitude of signal is amplified 242.8 times compared to the initial sensor input as shown in Fig. (11f). The signal strength is adequate for further process using two chips of LM324N. The signal after precision full-wave rectification (step I) is given in Fig. (11g). Through the reversed-phase proportional amplifier in block J, signal amplitude is magnified five times as the red wave shown in Fig. (11h). Then smoothed signal shown in Fig. (11i) is obtained after a passive low-pass filter in block K. To validate the effect of retardation of comparison circuit in step L, we made an independent simulation using sinusoid input. As shown in Fig. (11j), the output level jumped as the expected function.



(a) Circuits boards in debugging



(b) Field application test

Fig. (12). Debugging and testing of the proposed system.

Based on the analysis and simulation for the designed circuit, we made PCB control boards as shown in Fig. (12a). The bottom one is for 24 channels sensor signals input and amplification, as well as the control circuits. The top one is for actuator driving. After debugging and adjustment, the installed boards for spun yarn detection and coarse tow stopping have shown satisfying performance in preliminary filed application as shown in Fig. (12b).

7. CURRENT & FUTURE DEVELOPMENTS

The developed control system for spun yarn breakage detection and coarse tow stopping had been tested both in laboratory and on the linen wet spinning frames in some middle-sized textile enterprises of southeastern China. Currently, three major drawbacks have been discovered. Firstly, different batches of coarse tow occasionally affect the detection sensitivity of the system. Secondly, thermal drift lead to the change of signal amplification gain. Thirdly, high humidity and environmental electromagnetic interference cause

instable output of the system in long-time running. Future work will be aimed at solving the above problems. The amplification gain will be modified to be grouped level-adjustable. Cooling fins or low-power fan will be added to prevent unacceptable thermal drift. The components placement and wiring layout will be optimized to improve the anti-interference of the system.

CONFLICT OF INTEREST

The authors confirm that this article content has no conflict of interest.

ACKNOWLEDGEMENTS

This work was supported in part by the Science Fund for Creative Research Groups from the National Natural Science Foundation of China (No. 51221004) and the Program for Zhejiang Leading Team of Science and Technology Innovation (No. 2010R50036).

REFERENCES

- [1] H.S.S. Sharma, L. Whiteside, and K. Kernaghan, "Enzymatic treatment of flax fibre at the roving stage for production of wet-spun yarn," *Enzyme Microb. Technol.*, vol. 37, pp. 386-394, Sep. 2005.
- [2] W.B. Fraser, "On the theory of ring spinning," *Philos. T. R. Soc. A.*, vol. 342, pp. 439-468, Feb. 1993.
- [3] Z.G. Xia and W.L. Xu, "A review of ring staple yarn spinning method development and its trend prediction," *J. Nat. Fibres*, vol. 10, pp. 62-81, Jan. 2013.
- [4] C.I. Su and P.T. Lai, "Evaluating the unevenness of stretch-broken tow in tow-to-yarn direct spinning," *Fibers Polym.*, vol. 11, pp. 648-653, Jan. 2010.
- [5] G. Ozcelik and E. Kirtay, "Examination of the influence of selected fibre properties on yarn neppiness," *Fibres Text. East. Eur.* vol. 14, pp. 52-57, Sep. 2006.
- [6] L. James, "End breaks in the spinning and weaving of weavable singles yarns Part 1: End breaks in spinning," *Text. Res. J.* vol. 75, pp. 507-511, Jun. 2005.
- [7] A. Morita and S. Goyude, "Draft roller, spinning unit, spinning machine, and manufacturing method of spun yarn," U. S. Patent 13,490,842, June 4, 2011.
- [8] H. Sawada, "Core fiber detecting method and device in core yarn spinning," U. S. Patent 7,770,873, August 10, 2010.
- [9] N. Hildebrand, "Capacitive sensor for detecting fluctuations in the mass and/or diameter of elongated textile test material," U. S. Patent 5,530,368, June 25, 1996.
- [10] P. Corriea, E. Killian, G. Lowry, and S. Mulkey, "Thickness measuring system for nonconducting materials," U. S. Patent 5,138,268, August 11, 1992.
- [11] V. Carvalho, J.G. Pinto, J.L. Monteiro, R.M. Vasconcelos, and F.O. Soares, "Yarn parameterization based on mass analysis," *Sens. Actuators A. Phys.* vol. 115, pp. 540-548, Sep. 2004.
- [12] D.J. Li, "The research of broken filaments detection device on viscose filament yarn," In: *Proceedings of Computational Intelligence and Security Workshops*, Harbin, China, 2007, pp. 910-913.
- [13] İ. Süle, "Investigation of the effect of the yarn production properties and wavelength on the sensor signatures detected upon defect," *Sens. Actuators A. Phys.* Vol. 170, pp. 72-83, Sep. 2011.
- [14] F. Hoesel and F.J. Minter, "Apparatus on a spinning preparation machine for monitoring fiber material," U. S. Patent 7,644,474, January 12, 2010.
- [15] P. Hans, "Process and device for cleaning sensors of a yarn monitoring system," U. S. Patent 5,421,529, June 6, 1995.
- [16] E. Musa, "Line-laser-based yarn shadow sensing break sensor," *Opt. Lasers Eng.* vol. 49, pp. 313-317, Mar. 2011.
- [17] M. Okayasu and Y. Sato, "New experimental techniques for in-situ measurement of the damage characteristics of piezoelectric ceramics under high cycle fatigue testing," *Exp. Mech.* Vol. 52, pp. 1009-1020, Oct. 2012.

Received: September 22, 2014

Revised: November 03, 2014

Accepted: November 06, 2014

© Jin *et al.*; Licensee Bentham Open.

This is an open access article licensed under the terms of the Creative Commons Attribution Non-Commercial License (<http://creativecommons.org/licenses/by-nc/3.0/>) which permits unrestricted, non-commercial use, distribution and reproduction in any medium, provided the work is properly cited.